

Article

Investigation of Photocatalysis by Mesoporous Titanium Dioxide Supported on Glass Fibers as an Integrated Technology for Water Remediation

Cristina De Ceglie ^{1,†}, Sudipto Pal ^{2,*} , Sapia Murgolo ¹, Antonio Licciulli ² and Giuseppe Mascolo ^{1,*} 

¹ Istituto di Ricerca sulle Acque, Consiglio Nazionale delle Ricerche, Via F. De Blasio 5, 70132 Bari, Italy; cristina.deceglie@ba.irsa.cnr.it (C.D.C.); sapia.murgolo@ba.irsa.cnr.it (S.M.)

² Department of Innovation Engineering, University of Salento, Via Per Monteroni, 73100 Lecce, Italy; antonio.licciulli@unisalento.it

* Correspondence: sudipto.pal@unisalento.it (S.P.); giuseppe.mascolo@ba.irsa.cnr.it (G.M.)

† These authors contributed equally to this work.

Abstract: The photocatalytic efficiency of an innovative UV-light catalyst consisting of a mesoporous TiO₂ coating on glass fibers was investigated for the degradation of pharmaceuticals (PhACs) in wastewater effluents. Photocatalytic activity of the synthesized material was tested, for the first time, on a secondary wastewater effluent spiked with nine PhACs and the results were compared with the photolysis used as a benchmark treatment. Replicate experiments were performed in a flow reactor equipped with a UV radiation source emitting at 254 nm. Interestingly, the novel photocatalyst led to the increase of the degradation of carbamazepine and trimethoprim (about 2.2 times faster than the photolysis). Several transformation products (TPs) resulting from both the spiked PhACs and the compounds naturally occurring in the secondary wastewater effluent were identified through UPLC-QTOF/MS/MS. Some of them, produced mainly from carbamazepine and trimethoprim, were still present at the end of the photolytic treatment, while they were completely or partially removed by the photocatalytic treatment.

Keywords: mesoporous titania; glass fiber; photocatalysis; contaminants of emerging concern; high resolution mass spectrometry; transformation products



Citation: De Ceglie, C.; Pal, S.; Murgolo, S.; Licciulli, A.; Mascolo, G. Investigation of Photocatalysis by Mesoporous Titanium Dioxide Supported on Glass Fibers as an Integrated Technology for Water Remediation. *Catalysts* **2022**, *12*, 41. <https://doi.org/10.3390/catal12010041>

Academic Editor: Ewa Kowalska

Received: 26 November 2021

Accepted: 27 December 2021

Published: 31 December 2021

Publisher's Note: MDPI stays neutral with regard to jurisdictional claims in published maps and institutional affiliations.



Copyright: © 2021 by the authors. Licensee MDPI, Basel, Switzerland. This article is an open access article distributed under the terms and conditions of the Creative Commons Attribution (CC BY) license (<https://creativecommons.org/licenses/by/4.0/>).

1. Introduction

The presence of compounds of emerging concern (CECs) such as pharmaceuticals, pesticides, personal care products, and surfactants in secondary wastewater effluents poses a threat to the receiving water bodies and, consequently, to wildlife and human health. This risk has led to the publication of guidelines by the World Health Organization (WHO), Food and Agriculture Organization of the United Nations (FAO), and Environmental Protection Agency (EPA), in which chemical and microbiological parameters of the wastewaters are considered [1]. The guidelines have been periodically updated since 1973. CECs and some of their transformation products (TPs) are poorly removed by the activated sludge process in conventional wastewater treatment plants (WWTPs) and the long-term exposure to them could cause reproductive and hormonal disorders as potential health problems [2] and the increase of bacterial antibiotic resistance [3].

Chlorination and UV-C light-assisted disinfection methods are the most commonly used treatment technologies in WWTPs and they also affect the removal of different classes of micropollutants [4–9]. However, transportation, handling, and chemical hazards are the main disadvantages of the chlorination process, whereas wastewater turbidity and adverse photoreactivation limit the use of UV treatment technology. In this regard, advanced oxidation processes (AOPs) represent a more efficient alternative due to their versatility toward degrading organic and inorganic contaminants in water and on solid phases [5,10–13].

Among the AOPs, heterogeneous photocatalysis is promising for water treatment due to its versatility and it is also eco-friendly since no chemicals are directly required during the process [14–16]. The working principle of photocatalytic oxidation relies on the generation of strong oxidant and highly reactive species like hydroxyl radicals (OH^\bullet), irradiating the surface of a semiconductor with a light source having energy greater than its bandgap [17,18]. In a controlled reaction, the OH^\bullet radicals can completely mineralize the organic contaminants in water matrices. The advantages of using titanium dioxide (TiO_2) as a photocatalyst for the removal of CECs in water treatment are widely reported in the literature [17–19], concerning its high photo-stability and inertness in the chemical environment, wide availability, low cost and non-toxicity.

One of the most interesting challenges in water treatment is the synthesis of novel and efficient catalysts based on TiO_2 nanoparticles for the degradation of CECs in real secondary wastewater effluents. Although the activity of TiO_2 is higher in its powder form while performing photocatalysis in suspension, the recovery of the catalyst at the end of the oxidation process is very complex and cost-effective especially in a scaled-up system limiting its applicability [20]. In this perspective, the immobilization of TiO_2 catalyst on inert materials such as glass, silica, activated carbon, polymeric materials is preferable to the suspended TiO_2 as it facilitates the recovery of the catalyst at the end of the treatment and minimizes the traces of photocatalyst nanoparticles in the final treated waters [21–23]. Achievement of highly available active surfaces, the selection of the best support in terms of thermal and mechanical stability, or chemical inertness towards the catalyst, as well as the choice of the synthesis procedure are factors of primary importance in the developed immobilization technique. Porous substrates, such as activated carbon, diatomaceous earth, nanoclays, hollow glass spheres, and polymeric materials, are often used as supported catalysts due to their higher adsorption capacity [24]. In this context, the application of mesoporous TiO_2 in water remediation has been also investigated [25,26] However, there is a serious issue of using these kinds of materials since a sintering process is necessary to fix nanostructured TiO_2 coating to the substrate, which causes deformation and sometimes the loss of the porous structure [27]. In this context, glass fiber mats could be a good alternative due to their high flexibility, lightweight, high aspect ratio of the fibers, thermal stability, low cost and ability to remain stable under oxidation atmosphere and UV light irradiation [17,28,29].

In this work, a sol–gel dip coating technique was employed to obtain nanostructured TiO_2 coating on glass fiber mats. A pore generating agent was introduced in the sol preparation stage to achieve a mesoporous structure since TiO_2 coating often suffers low photocatalytic activity due to its lower surface area, especially when a highly crystalline phase is obtained by sintering the coating at high temperature. The mesoporous structure with a higher surface area increases the number of active sites on the catalyst surface that enhances the rate of photo-oxidation reaction thus improving the overall efficiency [30].

The present study aims to evaluate the effectiveness of photocatalysis employing a novel nanostructured and mesoporous TiO_2 coating on glass fiber mats for the removal of nine PhACs (carbamazepine, cetirizine, clarithromycin, climbazole, diclofenac, irbesartan, lidocaine, torsemide, and trimethoprim) spiked in a real secondary wastewater effluent, beside the removal of the naturally occurring CECs, as an integrated technology for water remediation. In addition, the identification of the transformation products (TPs), formed during both photolytic and photocatalytic treatments was also performed.

2. Results and Discussion

2.1. Mesoporous TiO_2 /Glass Fibers: Synthesis and Characterization

Figure 1 shows the XRD pattern of the mesoporous nanocrystalline TiO_2 film deposited on the glass fiber mat, which shows several well-resolved diffraction peaks corresponding to various reflection planes of the crystalline anatase phase of TiO_2 (JCPDS no. 84-1286) as indicated in the figure. The absence of any rutile peak indicates the formation of pure anatase nanocrystalline phase. The average particle size estimated from the (101) plane

of the XRD spectra using the Scherrer's equation ($D = k\lambda/\beta\cos\theta$, where D is the average crystallite size, k is the Scherrer constant (0.9), λ is the wavelength of the radiation source, β is the full line width at half-maxima of the (101) diffraction peak and θ is the angle of the corresponding diffraction peak) was found to be about 15 nm.

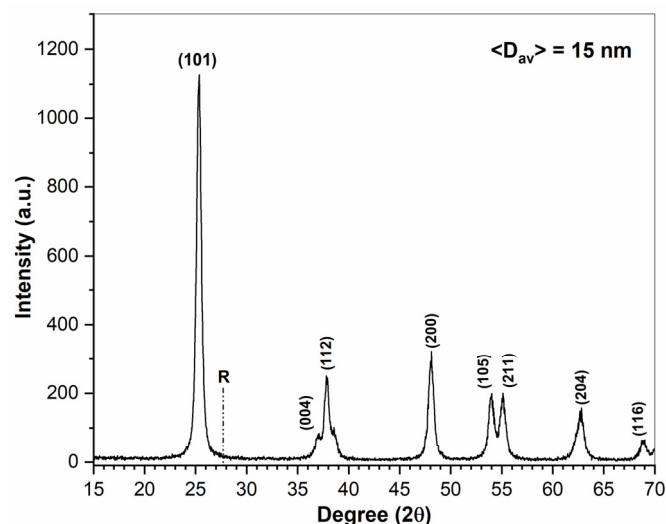


Figure 1. XRD pattern of the mesoporous TiO_2 coating on glass fibers.

The amount of TiO_2 loading on the glass fiber mats was estimated from the XRF spectra shown in Figure 2. As a comparison, the spectra of bare glass fiber is also shown. The appearance of a strong Ti peak indicates the presence of TiO_2 in the composite mat. The elemental distribution (Figure 2b) shows an almost homogeneous distribution of TiO_2 over the substrate. The average TiO_2 loading was estimated to be about 16% by weight.

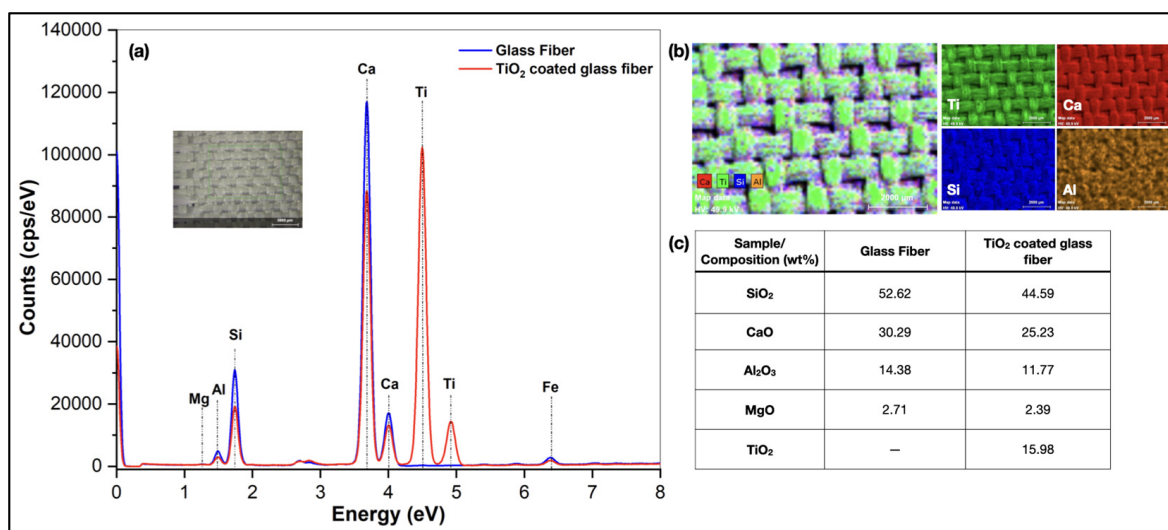


Figure 2. (a) XRF spectra of the TiO_2 coating on glass fiber. The inset shows real image of the TiO_2 coated glass fiber with the indicated area from where the spectrum was recorded; (b) elemental mapping of the major elements present; (c) estimation of TiO_2 loading on glass fiber.

The mesoporosity of the nanostructured film was analyzed by the BET surface area measurements. The specific surface area was calculated to be $61.2 \text{ m}^2/\text{g}$. Figure 3a shows the N_2 adsorption–desorption isotherm plot that corresponds to the typical type IV isotherm pattern with type H1 hysteresis. The adsorption branch shows a lower slope in the low relative pressure range (multilayer adsorption) followed by a sharp rise at a higher relative

pressure (pore condensation in mesopore), whereas the desorption branch follows a narrow hysteresis loop where the desorption branch is parallel to the adsorption branch, indicating the formation of a narrow distribution of uniform mesopores. This is reflected in Figure 3b, which shows the BJH pore size distribution plot calculated from the desorption branch of the isotherm, where a narrow pore size distribution with an average pore diameter of 5.57 nm is observed. This data confirms the formation of mesoporous structure in the coating material [31].

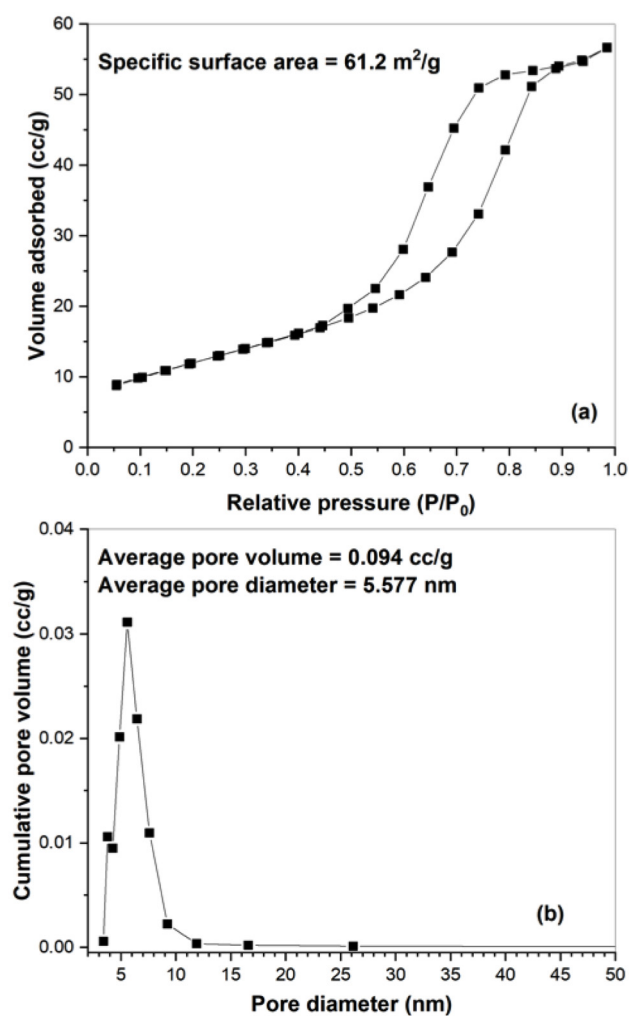


Figure 3. (a) N₂ adsorption-desorption isotherm and (b) BJH pore size distribution of the mesoporous TiO₂ coating. Specific surface area was calculated from the multilayer BET plot of the adsorption branch in the relative pressure of 0.05–0.30 range.

Morphological analysis was carried out to realize how TiO₂ nanoparticles are attached to the glass fiber surface. Figure 4a–d shows the FESEM micrographs of the mesoporous TiO₂ coating on the fibers at different magnifications. Every single fiber coated with TiO₂ nanoparticles is observed in Figure 4a, which is strongly supported by the presence of Ti in XRF spectra (Figure 2). More enlarged images are shown in Figure 4b–d, where the coating is clearly visible consisting of spherical TiO₂ nanoparticles. The broken part shows agglomerated nanoparticles, whereas the top smooth part shows a uniform coating with mesoporous nature, particularly in Figure 4d. This data confirms the strong attachment of the TiO₂ nanoparticles to the fiber surface. Moreover, due to the mesoporous structure, the coated surface became superhydrophilic showing water contact angle between 5 to 8° (data not shown) that would enhance the photocatalytic activity.

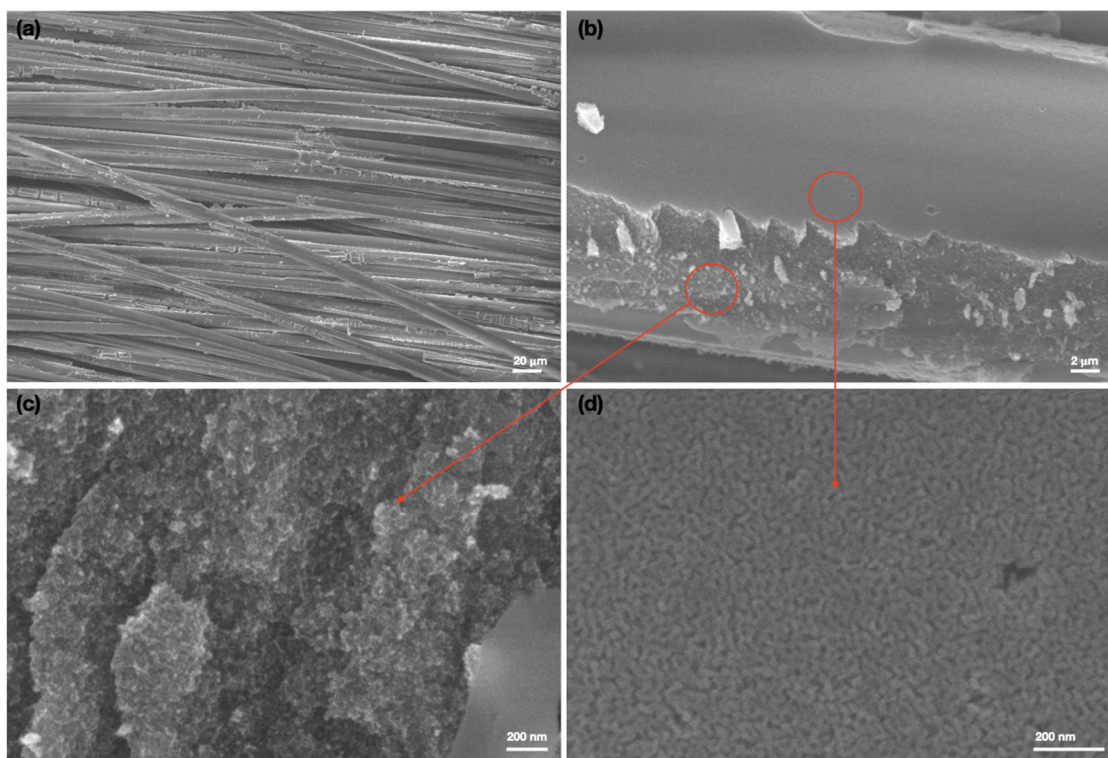


Figure 4. FESEM images of the mesoporous TiO₂ coating on glass fiber: (a) every single fiber coated with TiO₂ nanoparticles; (b–d) enlarged images showing the spherical TiO₂ nanoparticles.

2.2. Photocatalytic Degradation of Spiked PhACs

An up-flow reactor (0.5 L) equipped with a low-pressure mercury UV lamp emitting monochromatic UV radiation at a wavelength of 254 nm (40 W) was employed in recirculation mode for photolytic and photocatalytic experiments [32]. The volume of the treated solution was 1.2 L and each test was performed twice at a controlled temperature (30 °C). For the photocatalytic experiments, the catalyst fabric was wrapped around the quartz tube, which protects the UV lamp (Figure 5). Before starting the photocatalytic treatments, the catalyst fabric was exposed to a water up-flow of 6 L h⁻¹ for 30 min in order to verify the adsorption of CECs on the supported catalyst. Photolysis experiments with only UV light irradiation were performed as benchmark treatments. The secondary wastewater effluent used for the investigation was spiked with the target compounds (at a concentration of about 200 μg L⁻¹). The structures of the drugs studied are shown in Figure 6.

After exposure to the UV light, some compounds such as diclofenac and cetirizine were completely degraded, after 20 and 60 min of reaction time, respectively (data not shown). The phototransformation rate is strictly dependent on the nature of the compound, in particular, the presence in the structures of groups absorbing UV energy as for example conjugated double bonds and hetero-atoms. Diclofenac is well-known to be susceptible to direct photolysis [33,34] and cetirizine, showing a very complex structure, is more susceptible to fast UV degradation due to the several routes of fragmentation. The photochemical behavior of the other investigated PhACs that exhibited slower removal kinetics, mainly CBZ, IBS and TMP, is different. In Table 1 the kinetic constants (k , min⁻¹) obtained for each contaminant during both photolytic and photocatalytic treatments (performed in duplicate) are listed. As far as diclofenac, it was quickly removed during the photolysis and therefore it was not possible to investigate the performance of the catalyst.

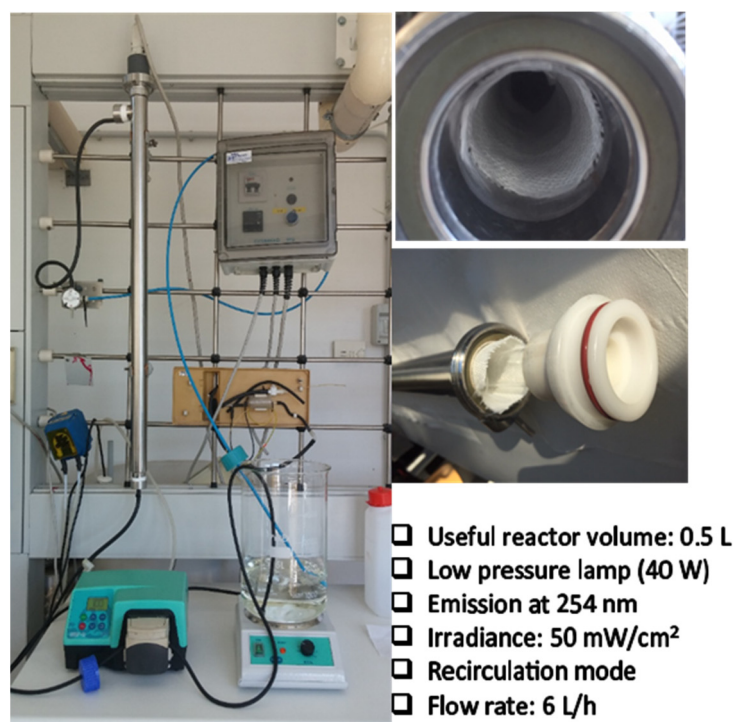


Figure 5. Photocatalytic system equipped with UV lamp, quartz tube and mesoporous titanium dioxide supported on glass fiber mats.

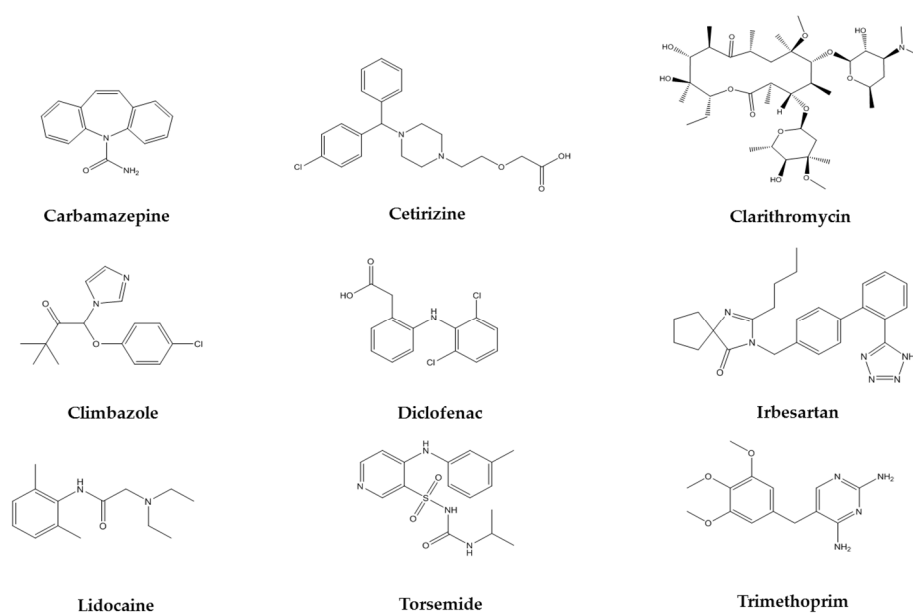


Figure 6. Chemical structures of the studied pharmaceuticals.

These results demonstrated that the compounds CBZ and TMP are the most recalcitrant to the photolytic treatment being the values of rate constants as the smallest ones (0.029 min^{-1} and 0.028 min^{-1} , respectively). CBZ and TMP are known for their slow photo-transformation rates [35] and consequently, their removal as well as the removal of formed TPs is important to increase water quality. In a recent paper, Paredes and colleagues investigated a novel catalyst based on immobilized TiO_2 on PVDF dual-layer hollow fiber membranes for the photo-transformation of eight target pharmaceuticals and they found that CBZ, TMP and metoprolol were more rapidly removed by photocatalysis compared to photolysis [36].

Table 1. First-order kinetic constants (k , min^{-1}) for spiked PhACs obtained during photolytic and photocatalytic treatments, treating secondary wastewater effluent.

Spiked PhACs	Elemental Composition	m/z (Da)	k (min^{-1})	
			Photolysis (Average \pm SD)	Photocatalysis Mesoporous TiO_2 on Glass Fibers (Average \pm SD)
CBZ	$\text{C}_{15}\text{H}_{12}\text{N}_2\text{O}$	237.1014	0.029 ± 0.001	0.068 ± 0.023
CTZ	$\text{C}_{21}\text{H}_{25}\text{N}_2\text{O}_3\text{Cl}$	389.1610	0.402 ± 0.066	0.289 ± 0.022
CLR	$\text{C}_{38}\text{H}_{69}\text{NO}_{13}$	748.4762	0.051 ± 0.004	0.061 ± 0.007
CLI	$\text{C}_{15}\text{H}_{17}\text{N}_2\text{O}_2\text{Cl}$	293.1050	0.233 ± 0.020	0.183 ± 0.011
DCF	$\text{C}_{14}\text{H}_{11}\text{NO}_2\text{Cl}_2$	296.0241	-	-
IBS	$\text{C}_{25}\text{H}_{28}\text{N}_6\text{O}$	429.2362	0.050 ± 0.001	0.059 ± 0.002
LDC	$\text{C}_{14}\text{H}_{22}\text{N}_2\text{O}$	235.1794	0.061 ± 0.002	0.065 ± 0.010
TOR	$\text{C}_{16}\text{H}_{20}\text{N}_4\text{O}_3\text{S}$	349.1306	0.081 ± 0.003	0.088 ± 0.011
TMP	$\text{C}_{14}\text{H}_{18}\text{N}_4\text{O}_3$	291.1439	0.028 ± 0.001	0.062 ± 0.014

According to Lian et al. [37], in wastewaters effluents, the photolabile species can be classified into five groups. IBS being included in the IV group (photochemically produced reactive intermediates combination-dominated group), was characterized by a slow degradation reaction with respect to the compounds belonging to the first three groups. CLI is considered moderately photo-susceptible while in the study of Kim et al. [38], clarithromycin is classified as a slow degrading pharmaceutical. It seems that the presence of dissolved organic matters promotes photodegradation of lidocaine and torsemide

The application of the mesoporous titanium dioxide supported on glass fibers allowed for increasing the photo-transformation rate of CBZ and TMP compared to the photolytic treatment of about 2.2 times. For the other tested PhACs the kinetic constants were slightly higher in presence of the novel photocatalyst except for CTZ and CLI for which a decrease in removal was observed during the photocatalytic process (Table 1).

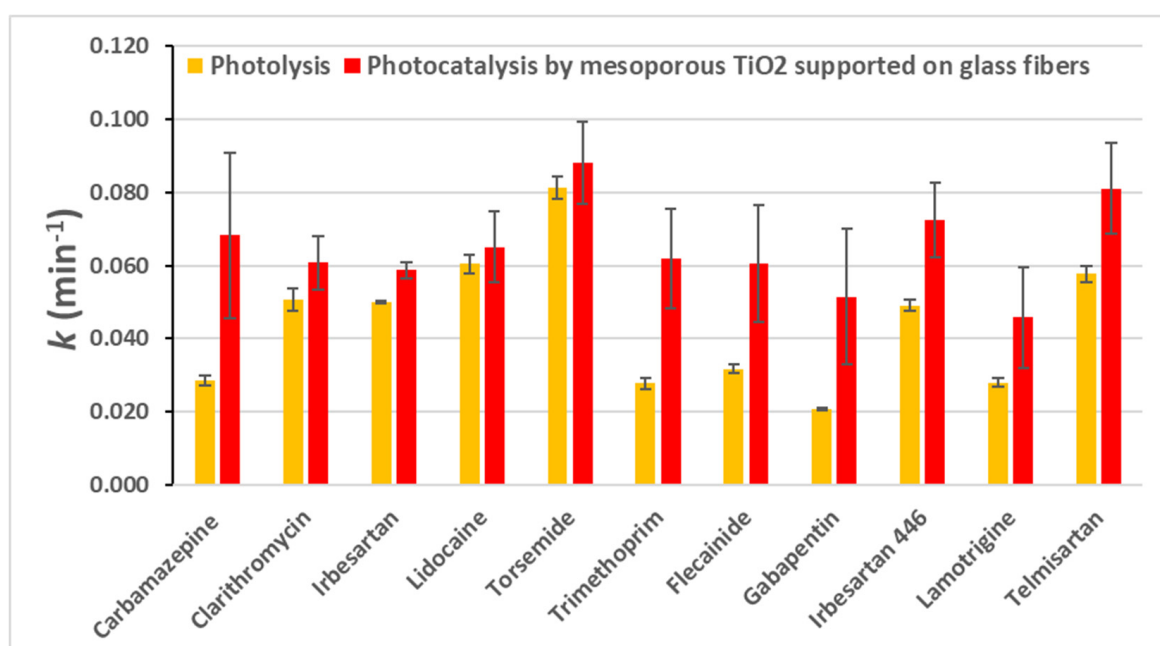
2.3. Photocatalytic Degradation of Naturally Occurring PhACs

The performance of the novel catalyst was investigated for the removal of CECs naturally present in the secondary wastewater effluent. In this perspective, a targeted screening was performed employing the AB SCIEX software for both compound identification and trend detection. A group of eight additional PhACs was detected in the secondary wastewater effluent including candesartan, flecainide, gabapentin, irbesartan 446, lamotrigine, niflumic acid, telmisartan, and venlafaxine. The concentration of such CECs was measured between 0.5 and 5 $\mu\text{g}/\text{L}$. For five of these compounds (flecainide, gabapentin, irbesartan 446, lamotrigine and telmisartan), it was possible to measure the pseudo first-order kinetic constant during the UV-based treatments (with and without the photocatalyst) while candesartan, niflumic acid, and venlafaxine were quickly removed during the treatment by UV light alone (Table 2).

Average k values for all the detected substances (Table 2) were higher for photocatalysis, so the presence of the mesoporous TiO_2 -based photocatalyst increased their photodegradation. In Figure 7, the main results relative to photolysis and photocatalysis for both the spiked and the naturally occurring contaminants, in terms of k (min^{-1}) values, are summarized. For each CEC, the average k value and the standard deviation are reported.

Table 2. First-order kinetic constants (k , min^{-1}) for naturally occurring PhACs obtained during photolytic and photocatalytic treatments, treating secondary wastewater effluent.

PhACs	Elemental Composition	m/z (Da)	k (min^{-1})	
			Photolysis (Average \pm SD)	Photocatalysis Mesoporous TiO_2 on Glass Fibers (Average \pm SD)
Flecainide	$\text{C}_{17}\text{H}_{20}\text{N}_2\text{O}_3\text{F}_6$	415.1440	0.032 ± 0.001	0.061 ± 0.016
Gabapentin	$\text{C}_9\text{H}_{17}\text{NO}_2$	172.1331	0.021 ± 0.001	0.052 ± 0.019
Irbesartan 446	$\text{C}_{25}\text{H}_{30}\text{N}_6\text{O}_2$	447.2486	0.049 ± 0.001	0.073 ± 0.011
Lamotrigine	$\text{C}_9\text{H}_7\text{N}_5\text{Cl}_2$	256.0150	0.028 ± 0.001	0.046 ± 0.014
Telmisartan	$\text{C}_{33}\text{H}_{30}\text{N}_4\text{O}_2$	515.2428	0.058 ± 0.002	0.081 ± 0.013

**Figure 7.** Identification of phototransformation products.

The software MetabolitePilot allowed for the identification of 26 transformation products formed from the spiked PhACs (Table S1). In the attempt to propose a chemical structure for the detected TPs, the data deriving from a deep bibliography research were combined with the accurate MS and MS/MS information achieved with the UPLC-QTOF/MS/MS analyses. Several detected TPs are already known in literature and the relative references (mentioned in Table S1) were used as a suggestion for structure elucidation [39,40]. The main difficulty in the attribution of the correct structure is the presence of numerous isomers for some TPs (for example CBZ-5 and CBZ-6). These isomers having the same accurate mass, show different retention times because they only differ for the position of a specific group, for example an OH group. If the analyte intensity is too low and MS/MS spectra are of poor quality, it is not possible to obtain a confident attribution. Among the six TPs of carbamazepine ($[\text{M}+\text{H}]^+$ 237.1014), five of them were discussed in detail by Calza et al., Franz et al. and Martinez-Piernas et al. [39–41]. Only CBZ-3, at m/z value of 241.0601, was considered as a new TP because, at present, its formation was not revealed in other scientific works. As far as clarithromycin ($[\text{M}+\text{H}]^+$ 748.4762) all the detected TPs were described by Calza et al. [39] and Buchicchio et al. [42]

Interestingly, for climbazole ($[\text{M}+\text{H}]^+$ 293.1050) the TP with m/z 167.1175 showed a MS/MS spectrum identical to that acquired by Castro et al. [43] and it results from

the cleavage of the ether bond. According to the identification confidence levels of Schymanski et al. [44] the molecular structure of TP CLI-1 can be assigned as a probable structure (Level 2a). Two additional CLI-TPs were revealed for the first time in this work, the first one at m/z of 247.1448 (CLI-2) and the second one, at m/z 338.0887 (CLI-3, a nitro-derivative of climbazole).

The MS/MS spectrum of CLI-3 revealed a fragment at m/z 69.0456 that is present only in the MS/MS spectrum of climbazole and that corresponds to the protonated imidazole ($C_3H_5N_2^+$). The mass shift between the TP (m/z 338.0887) and the parent compound (m/z 293.1050) was 44.98 Da corresponding to nitration, so the empirical formula $C_{15}H_{16}N_3O_4Cl$ was attributed to this product, identified as nitro-climbazole. The observation of the protonated imidazole in the MS/MS spectrum could be proof of the nitration of the phenyl ring. This kind of modification was discussed by Nelieu et al. [45] during the photodegradation of monuron in an aqueous solution. In addition to IBS-1 and IBS-2 [46,47] another TP of irbesartan at m/z 445.2338 obtaining from the addition of one -OH group to the parent compound ($[M+H]^+$ 429.2362) was detected and its probable structure is illustrated in the Table S1.

For lidocaine ($[M+H]^+$ 235.1794) three new TPs were identified LDC-1, LDC-2, and LDC-3 at 233.1647 m/z , 283.1656 m/z , and 299.1603 m/z , respectively, and their chemical structures were attributed with a high confidence level. The proposed structures were suggested by the detailed study of Rayaroth et al. [48] about the degradation mechanism of lidocaine by photocatalysis that involves the hydroxyl radicals as major reactive species.

The transformation products of torsemide ($[M+H]^+$ 349.1306) in the aquatic environment were investigated in the recent work of Lege et al. [49]. The article focuses on the degradation products derived from various treatments included photo-transformation; 4 photolysis TPs (TP 364b, TP 362, TP 258 and TP 393) were identified by Lege and coworkers, the first three TPs with a confidence level 2 and the last one with a confidence level 4. For TP 364 three isomers (TP 364 a, b, c) with molecular formula $C_{16}H_{20}N_4O_4S$ were detected after the different degradation studies. Only TP 364b (exact monoisotopic mass of $[M+H]^+$: 365.1278 m/z) was present after each kind of treatment, thus revealing the importance of this TP in the degradation pathway of this drug. The three isomers represent the hydroxylation products of torsemide and they differ in the hydroxylation site [49].

In the present work, the molecular ion at 365.1264 m/z was detected after photodegradation experiments (TOR-2) and the MS/MS spectrum matches that of TP 364b. The molecular ion at 363.1112 m/z (TOR-1) was the same as TP 362, deriving from ketone formation. The formation of TP 258 after photolysis was of minor significance compared to the other TPs in the investigation of Lege et al. [49]; this type of by-product was not detected in the present study. Finally, the TP 393 (exact monoisotopic mass of $[M+H]^+$: 394.1180 m/z), attributed as nitro-torsemide, was also recognized in our reaction samples. Unlike Lege et al., we succeeded in identifying the TP with a confidence level of 2 (TOR-3) because of the good quality of the acquired MS/MS spectrum and the high intensity of the fragments.

For trimethoprim ($[M+H]^+$ 291.1439) the detected TPs were already identified by Paredes et al. [36]. No degradation products of cetirizine and diclofenac having a significant removal trend were detected in the present investigation. In Figure 8, the time profiles of the most representative transformation product for three (CBZ, CLR, TMP) spiked compounds were reported. Most of the detected TPs showed a bell-shape trend (a more comprehensive view of TPs time profiles is present in Figures S1–S7) and four different trends were noted: (i) the photolytic treatment generates a TP with higher intensity respect to photocatalytic treatment, with a delay in the removal of the compound (CBZ-5 and CLR-1, Figure 8); (ii) the TP increases during photolytic treatment and it seems to accumulate along reaction time while negligible formation is observed during photocatalysis (TMP-1, Figure 8); (iii) no differences are observed between photolysis and photocatalysis (IBS-3, Figure S4); (iv) at first, a higher amount of the TP is observed during the photocatalytic treatment but, then, the decrease is similar for both the treatments (CLR-3, Figure S2).

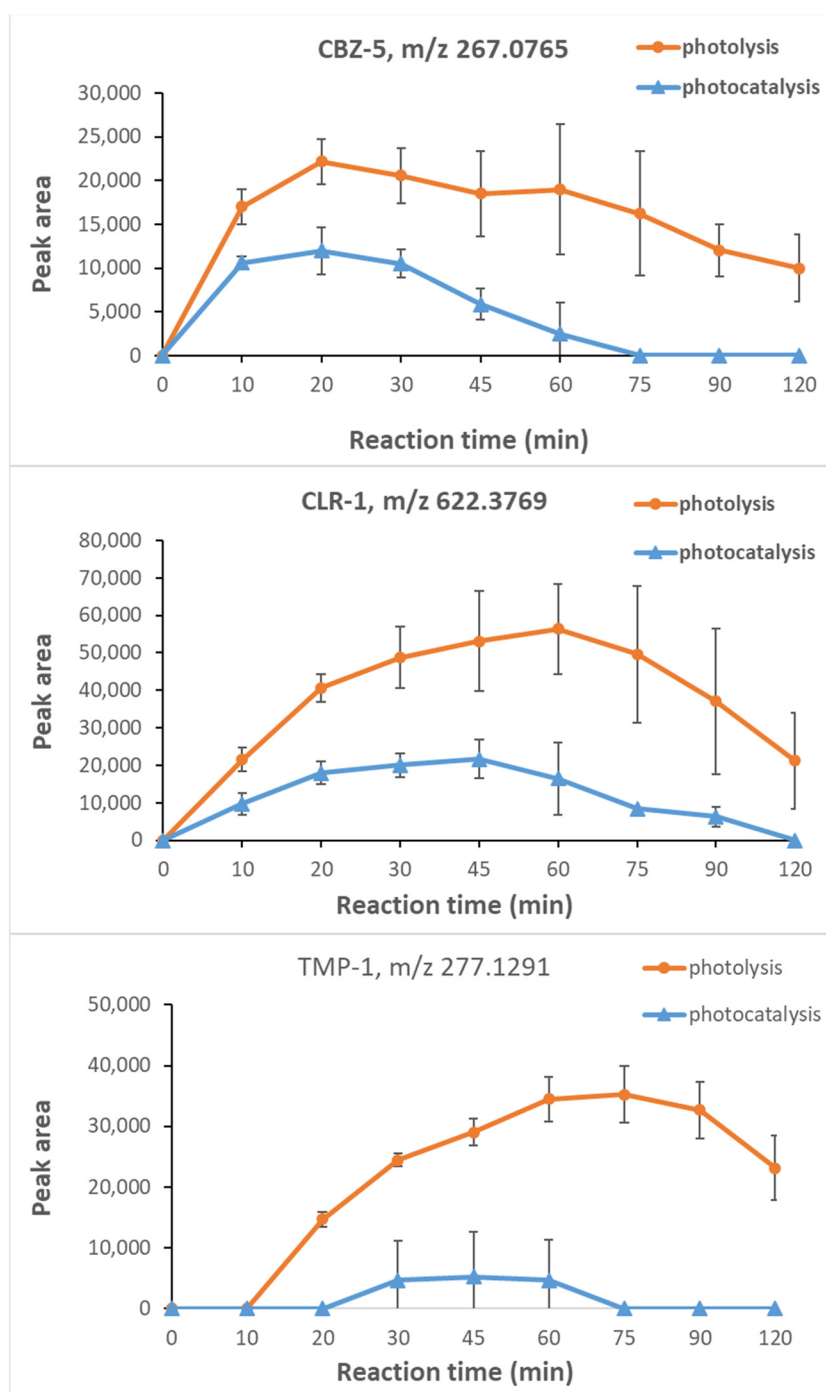


Figure 8. Time profiles of the TPs CBZ-5, CLR-1, and TMP-1 during photolysis and photocatalysis with mesoporous TiO₂ coated on glass fibers, using secondary wastewater effluent.

Among the previously described trends, it is worth noting the second one, in fact, in other works such as that of Paredes et al. [36], a similar behaviour was not highlighted. Considering the first trend typology, different TPs are still present in the reaction sample after the end of the photolysis while they were fast removed during photocatalysis: i.e., CBZ-5 and CBZ-6, CLR-1, CLR-4, CLI-2, TOR-1 and, interestingly, all the detected TPs of trimethoprim.

3. Materials and Methods

3.1. Selection of Pharmaceutical Compounds

Nine pharmaceutical compounds not completely removed in conventional wastewater treatment and usually detected in secondary wastewater effluents at trace concentrations (i.e., $\mu\text{g/L}$ – ng/L) were selected as target contaminants to investigate the efficiency of the novel photocatalyst: carbamazepine (CBZ), cetirizine (CTZ), clarithromycin (CLR), climbazole (CLI), diclofenac (DCF), irbesartan (IBS), lidocaine (LDC), torsemide (TOR), and trimethoprim (TMP). All the listed compounds were spiked in a real secondary wastewater effluent at a final concentration ranging between 100 and 200 $\mu\text{g/L}$. The effluent was taken from a self-forming dynamic membrane bioreactor treating municipal wastewater and characterized according to standard methods. All chemicals were purchased from Sigma–Aldrich as well as the solvents used for chromatographic analyses and for preparing standard solutions, e.g., acetonitrile, methanol and formic acid (UPLC grade).

3.2. Synthesis and Characterization of the Mesoporous TiO_2 Coating on Glass Fiber

Mesoporous TiO_2 coating was deposited on the glass fiber mats by sol–gel method using the dip technique. The TiO_2 sol (containing 5% of TiO_2 by weight in ethanol) was prepared by hydrolysis-condensation of titanium isopropoxide (TTIP, Sigma–Aldrich, St. Louis, MO, USA, 97%) in presence of hydrochloric acid (HCl, Alfa-Aesar 37%) and deionized water (Millipore Milli Q). The triblock copolymer, Pluronic P123 ($\text{PEO}_{20}\text{PPO}_{70}\text{PEO}_{20}$, average $M_{\text{av}} \sim 5800$, Sigma–Aldrich) was used as a mesopore generating template. The molar ratios of the reagents were $\text{TTIP}:\text{HCl}:\text{H}_2\text{O}:\text{P123} = 1:0.5:4:0.0125$. At first, P123 was dissolved in the appropriate amount of ethanol followed by the addition of TTIP drop-wise to the above solution. After homogeneous mixing of the solution, the required amount of HCl was diluted with water and drop-wise added. The sol was left under stirring for several hours to complete the hydrolysis-condensation reaction. The as prepared sol aged for one day before the coating application. Commercially available glass fiber mats (approx. composition 52% SiO_2 , 30% CaO , 14% Al_2O_3 , 2% MgO) were used as the substrate to deposit the TiO_2 coating. The glass fiber mats were cut into 30×20 cm size and preliminary treated at 500 °C in the air for 1 h to decompose any organic binder present. The organic-free glass fiber mats were coated with the TiO_2 sol by dip-coating method at a withdrawal speed of 20 cm/min. After the coating deposition, the mats were kept in an oven at 65 °C for one night to gently dry the coated film and avoid any unwanted cracks. Sintering and template removal took place at 500 °C for 2 h in the air at the heating rate of 1 °C/min and maintaining a similar cooling rate as well, after which the mesoporous nanocrystalline TiO_2 coating was formed on the glass fiber mat.

3.3. Microstructural Characterization

Nanocrystalline phase formation of TiO_2 in the coated film was investigated by X-ray diffraction (XRD) analysis that performed with a Rigaku Ultima X-ray diffractometer using $\text{Cu K}\alpha$ radiation ($\lambda = 1.5406 \text{ \AA}$) operating at 40 kV/30 mA with the step size of 0.02° . Morphological characterization of the coating was carried out on a Zeiss Sigma VP field emission scanning electron microscope (FESEM). The amount of TiO_2 loading on the glass fiber mat was determined by X-ray fluorescence spectroscopy (XRF). It was performed with a Bruker M4 Tornado (Bruker Nano Germany) X-ray fluorescence spectrometer operating at 50 kV/600 μA (30 W) equipped with X-Flash silicon drift detector. The measurements were performed in area mode (approx. 35 mm^2) and the elemental quantification was estimated from the average of five measurements.

3.4. PhACs Concentration Measurements

The concentration of the selected PhACs during photolytic and photocatalytic treatments was determined using a high-resolution mass spectrometer, TripleTOF 5600+ system (AB Sciex), coupled to a liquid chromatographic system, Ultimate 3000 (Thermo Fisher Scientific, Waltham, MA, USA), by means of a duo-spray ion source operated in positive

electrospray (ESI) mode. All MS analyses were acquired with an acquisition method based on double experiments, i.e., full-scan survey TOF-MS and IDA (information dependent acquisition) experiment. 50 μ L samples were injected and eluted with a binary gradient consisting of 0.1% formic acid in water (solvent A) and 0.1% formic acid in MeCN (solvent B), employing a Waters BEH C18 column (2.1 \times 150 mm, 1.7 μ m) operating at a flow of 0.200 mL/min. Before LC/MS analysis, carbamazepine D10 was added as an internal standard to each sample at a final concentration of 10 μ g/L. AB Sciex software was used for data processing, i.e., SciexOS 1.2, LibraryView 1.0.2 and MetabolitePilot 1.5. ChemBioDraw Ultra 13.0 was used for TPs structure elucidation.

4. Conclusions

A novel photocatalytic system consisting of mesoporous titanium dioxide supported on glass fibers as the catalyst substrate in a UV reactor arrangement has been developed to remove the pharmaceutical contaminants. Highly crystalline and nanostructured mesoporous TiO₂ coatings with a high surface area were successfully fixed to the fiber surfaces after the sintering process. The microstructural analysis confirmed the formation of mesoporosity in the coating matrix. The large exposed area of the glass fiber mat allowed the fast photo-oxidation rate compared to the photolysis. The degradation study carried out with the new catalyst support showed that it was effective not only in the removal of most of the PhACs investigated, with particular reference to carbamazepine and trimethoprim, but also in the abatement of their TPs. The strong attachment of the TiO₂ coating to the fiber surfaces showed the reusability of the supported catalyst without spending the effort to recover it after the photocatalytic reaction. This simple coating strategy can be extended to either other suitable catalyst support or to modify the starting solution to make it visible light active (e.g., by doping with Ag, Cu, Au, Fe₂O₃, etc.).

Supplementary Materials: The following are available online at <https://www.mdpi.com/article/10.3390/catal12010041/s1>, Figure S1. Time profiles of CBZ TPs during photolysis and photocatalysis with mesoporous TiO₂ coated on glass fibers, using secondary wastewater effluent, Figure S2. Time profiles of CLR TPs during photolysis and photocatalysis with mesoporous TiO₂ coated on glass fibers, using secondary wastewater effluent, Figure S3. Time profiles of CLI TPs during photolysis and photocatalysis with mesoporous TiO₂ coated on glass fibers, using secondary wastewater effluent, Figure S4. Time profiles of IBS TPs during photolysis and photocatalysis with mesoporous TiO₂ coated on glass fibers, using secondary wastewater effluent, Figure S5. Time profiles of LDC TPs during photolysis and photocatalysis with mesoporous TiO₂ coated on glass fibers, using secondary wastewater effluent, Figure S6. Time profiles of TOR TPs during photolysis and photocatalysis with mesoporous TiO₂ coated on glass fibers, using secondary wastewater effluent, Figure S7. Time profiles of TMP TPs during photolysis and photocatalysis with mesoporous TiO₂ coated on glass fibers, using secondary wastewater effluent, Table S1. List of transformation products of the *spiked compounds* detected by suspect screening in photolytic and photocatalytic experiments (mesoporous TiO₂ supported on glass fibers), treating secondary wastewater effluent.

Author Contributions: Conceptualization, C.D.C. and S.P.; methodology, C.D.C., S.P. and S.M.; software, C.D.C., S.M.; validation, C.D.C., S.M. and G.M.; investigation, C.D.C., S.P. and S.M.; resources, C.D.C., S.P. and S.M.; data curation, C.D.C., S.M.; writing—original draft preparation, C.D.C., S.P. and S.M.; writing—review and editing, C.D.C., S.P., S.M., A.L. and G.M.; visualization, A.L., G.M.; supervision, A.L., G.M. All authors have read and agreed to the published version of the manuscript.

Funding: This research received no external funding.

Data Availability Statement: The data, either raw or processed required to reproduce these research works cannot be shared at this time as the data also form part of an ongoing study.

Acknowledgments: The authors thank to Donato Cannoletta for performing the XRD measurements and Fabio Marzo for providing the FESEM measurements.

Conflicts of Interest: The authors declare no conflict of interest.

References

1. Jaramillo, M.F.; Restrepo, I. Wastewater Reuse in Agriculture: A Review about Its Limitations and Benefits. *Sustainability* **2017**, *9*, 1734. [CrossRef]
2. Gonsioroski, A.; Mourikes, V.E.; Flaws, J.A. Endocrine Disruptors in Water and Their Effects on the Reproductive System. *Int. J. Mol. Sci.* **2020**, *21*, 1929. [CrossRef]
3. Webb, S.; Ternes, T.; Gibert, M.; Olejniczak, K. Indirect Human Exposure to Pharmaceuticals via Drinking Water. *Toxicol. Lett.* **2003**, *142*, 157–167. [CrossRef]
4. Mezzanotte, V.; Antonelli, M.; Citterio, S.; Nurizzo, C. Wastewater Disinfection Alternatives: Chlorine, Ozone, Peracetic Acid, and UV Light. *Water Environ. Res.* **2007**, *79*, 2373–2379. [CrossRef] [PubMed]
5. Patel, M.; Kumar, R.; Kishor, K.; Mlsna, T.; Pittman, C.U.; Mohan, D. Pharmaceuticals of Emerging Concern in Aquatic Systems: Chemistry, Occurrence, Effects, and Removal Methods. *Chem. Rev.* **2019**, *119*, 3510–3673. [CrossRef]
6. Lopez, A.; Mascolo, G.; Földényi, R.; Passino, R. Disinfection By-Products Formation during Hypochlorination of Isoproturon Contaminated Groundwater. *Water Sci. Technol.* **1996**, *34*, 351–358. [CrossRef]
7. Lopez, A.; Mascolo, G.; Tiravanti, G.; Passino, R. Degradation of Herbicides (Ametryn and Isoproturon) during Water Disinfection by Means of Two Oxidants (Hypochlorite and Chlorine Dioxide). *Water Sci. Technol.* **1997**, *35*, 129–136. [CrossRef]
8. Lopez, A.; Mascolo, G.; Detomaso, A.; Lovecchio, G.; Villani, G. Temperature Activated Degradation (Mineralization) of 4-Chloro-3-Methyl Phenol by Fenton's Reagent. *Chemosphere* **2005**, *59*, 397–403. [CrossRef]
9. Mascolo, G.; Lopez, A.; Passino, R.; Ricco, G.; Tiravanti, G. Degradation of Sulphur Containing S-Triazines during Water Chlorination. *Water Res.* **1994**, *28*, 2499–2506. [CrossRef]
10. Wang, S.; Wang, J. Activation of Peroxymonosulfate by Sludge-Derived Biochar for the Degradation of Triclosan in Water and Wastewater. *Chem. Eng. J.* **2019**, *356*, 350–358. [CrossRef]
11. Yang, X.; Sun, J.; Fu, W.; Shang, C.; Li, Y.; Chen, Y.; Gan, W.; Fang, J. PPCP Degradation by UV/Chlorine Treatment and Its Impact on DBP Formation Potential in Real Waters. *Water Res.* **2016**, *98*, 309–318. [CrossRef]
12. De la Cruz, N.; Esquius, L.; Grandjean, D.; Magnet, A.; Tungler, A.; de Alencastro, L.F.; Pulgarín, C. Degradation of Emergent Contaminants by UV, UV/H₂O₂ and Neutral Photo-Fenton at Pilot Scale in a Domestic Wastewater Treatment Plant. *Water Res.* **2013**, *47*, 5836–5845. [CrossRef] [PubMed]
13. Pizzigallo, M.D.R.; Ruggiero, P.; Crecchio, C.; Mascolo, G. Oxidation of Chloroanilines at Metal Oxide Surfaces. *J. Agric. Food Chem.* **1998**, *46*, 2049–2054. [CrossRef]
14. Ibhaddon, A.O.; Fitzpatrick, P. Heterogeneous Photocatalysis: Recent Advances and Applications. *Catalysts* **2013**, *3*, 189–218. [CrossRef]
15. Emerging Contaminants from Industrial and Municipal Waste. Available online: <https://www.springerprofessional.de/en/emerging-contaminants-from-industrial-and-municipal-waste/2873406> (accessed on 17 December 2021).
16. Raja, P.; Bozzi, A.; Jardim, W.F.; Mascolo, G.; Renganathan, R.; Kiwi, J. Reductive/Oxidative Treatment with Superior Performance Relative to Oxidative Treatment during the Degradation of 4-Chlorophenol. *Appl. Catal. B Environ.* **2005**, *59*, 249–257. [CrossRef]
17. Pasini, S.M.; Valério, A.; Yin, G.; Wang, J.; de Souza, S.M.A.G.U.; Hotza, D.; de Souza, A.A.U. An Overview on Nanostructured TiO₂-Containing Fibers for Photocatalytic Degradation of Organic Pollutants in Wastewater Treatment. *J. Water Process Eng.* **2021**, *40*, 101827. [CrossRef]
18. Yuan, R.; Zhu, Y.; Zhou, B.; Hu, J. Photocatalytic Oxidation of Sulfamethoxazole in the Presence of TiO₂: Effect of Matrix in Aqueous Solution on Decomposition Mechanisms. *Chem. Eng. J.* **2019**, *359*, 1527–1536. [CrossRef]
19. Murgolo, S.; De Ceglie, C.; Di Iaconi, C.; Mascolo, G. Novel TiO₂-Based Catalysts Employed in Photocatalysis and Photoelectrocatalysis for Effective Degradation of Pharmaceuticals (PhACs) in Water: A Short Review. *Curr. Opin. Green Sustain. Chem.* **2021**, *30*, 100473. [CrossRef]
20. Pal, S.; Laera, A.M.; Licciulli, A.; Catalano, M.; Taurino, A. Biphasic TiO₂ Microspheres with Enhanced Photocatalytic Activity. *Ind. Eng. Chem. Res.* **2014**, *53*, 7931–7938. [CrossRef]
21. Byrne, C.; Subramanian, G.; Pillai, S.C. Recent Advances in Photocatalysis for Environmental Applications. *J. Environ. Chem. Eng.* **2018**, *6*, 3531–3555. [CrossRef]
22. Rachel, A.; Subrahmanyam, M.; Boule, P. Comparison of Photocatalytic Efficiencies of TiO₂ in Suspended and Immobilised Form for the Photocatalytic Degradation of Nitrobenzenesulfonic Acids. *Appl. Catal. B Environ.* **2002**, *37*, 301–308. [CrossRef]
23. Kim, D.S.; Park, Y.S. Photocatalytic Decolorization of Rhodamine B by Immobilized TiO₂ onto Silicone Sealant. *Chem. Eng. J.* **2006**, *116*, 133–137. [CrossRef]
24. Padmanabhan, S.K.; Pal, S.; Ul Haq, E.; Licciulli, A. Nanocrystalline TiO₂-Diatomite Composite Catalysts: Effect of Crystallization on the Photocatalytic Degradation of Rhodamine B. *Appl. Catal. A Gen.* **2014**, *485*, 157–162. [CrossRef]
25. Yacou, C.; Smart, S.; Diniz da Costa, J.C. Mesoporous TiO₂ Based Membranes for Water Desalination and Brine Processing. *Sep. Purif. Technol.* **2015**, *147*, 166–171. [CrossRef]
26. Akhavan, O.; Ghaderi, E. Self-Accumulated Ag Nanoparticles on Mesoporous TiO₂ Thin Film with High Bactericidal Activities. *Surf. Coat. Technol.* **2010**, *204*, 3676–3683. [CrossRef]

27. Hofstadler, K.; Bauer, R.; Novalic, S.; Heisler, G. New Reactor Design for Photocatalytic Wastewater Treatment with TiO₂ Immobilized on Fused-Silica Glass Fibers: Photomineralization of 4-Chlorophenol. *Environ. Sci. Technol.* **1994**, *28*, 670–674. [[CrossRef](#)] [[PubMed](#)]
28. Fukugaichi, S. Fixation of Titanium Dioxide Nanoparticles on Glass Fiber Cloths for Photocatalytic Degradation of Organic Dyes. *ACS Omega* **2019**, *4*, 15175–15180. [[CrossRef](#)] [[PubMed](#)]
29. Chen, L.; Yang, S.; Mäder, E.; Ma, P.-C. Controlled Synthesis of Hierarchical TiO₂ Nanoparticles on Glass Fibres and Their Photocatalytic Performance. *Dalton Trans.* **2014**, *43*, 12743–12753. [[CrossRef](#)]
30. Petronella, F.; Truppi, A.; Dell'Edera, M.; Agostiano, A.; Curri, M.L.; Comparelli, R. Scalable Synthesis of Mesoporous TiO₂ for Environmental Photocatalytic Applications. *Materials* **2019**, *12*, 1853. [[CrossRef](#)] [[PubMed](#)]
31. Licciulli, A.; Riccardis, A.D.; Pal, S.; Nisi, R.; Mele, G.; Cannoletta, D. Ethylene Photo-Oxidation on Copper Phthalocyanine Sensitized TiO₂ Films under Solar Radiation. *J. Photochem. Photobiol. A Chem.* **2017**, *346*, 523–529. [[CrossRef](#)]
32. Murgolo, S.; Yargeau, V.; Gerbasi, R.; Visentin, F.; El Habra, N.; Ricco, G.; Lacchetti, I.; Carere, M.; Curri, M.L.; Mascolo, G. A New Supported TiO₂ Film Deposited on Stainless Steel for the Photocatalytic Degradation of Contaminants of Emerging Concern. *Chem. Eng. J.* **2017**, *318*, 103–111. [[CrossRef](#)]
33. Carlson, J.C.; Stefan, M.I.; Parnis, J.M.; Metcalfe, C.D. Direct UV Photolysis of Selected Pharmaceuticals, Personal Care Products and Endocrine Disruptors in Aqueous Solution. *Water Res.* **2015**, *84*, 350–361. [[CrossRef](#)] [[PubMed](#)]
34. Homem, V.; Santos, L. Degradation and Removal Methods of Antibiotics from Aqueous Matrices—A Review. *J. Environ. Manag.* **2011**, *92*, 2304–2347. [[CrossRef](#)] [[PubMed](#)]
35. Afonso-Olivares, C.; Fernández-Rodríguez, C.; Ojeda-González, R.J.; Sosa-Ferrera, Z.; Santana-Rodríguez, J.J.; Rodríguez, J.M.D. Estimation of Kinetic Parameters and UV Doses Necessary to Remove Twenty-Three Pharmaceuticals from Pre-Treated Urban Wastewater by UV/H₂O₂. *J. Photochem. Photobiol. A Chem.* **2016**, *329*, 130–138. [[CrossRef](#)]
36. Paredes, L.; Murgolo, S.; Dzinun, H.; Dzarfan Othman, M.H.; Ismail, A.F.; Carballa, M.; Mascolo, G. Application of Immobilized TiO₂ on PVDF Dual Layer Hollow Fibre Membrane to Improve the Photocatalytic Removal of Pharmaceuticals in Different Water Matrices. *Appl. Catal. B Environ.* **2019**, *240*, 9–18. [[CrossRef](#)]
37. Lian, L.; Yan, S.; Zhou, H.; Song, W. Overview of the Phototransformation of Wastewater Effluents by High-Resolution Mass Spectrometry. *Environ. Sci. Technol.* **2020**, *54*, 1816–1826. [[CrossRef](#)]
38. Kim, I.; Tanaka, H. Photodegradation Characteristics of PPCPs in Water with UV Treatment. *Environ. Int.* **2009**, *35*, 793–802. [[CrossRef](#)] [[PubMed](#)]
39. Calza, P.; Medana, C.; Padovano, E.; Giancotti, V.; Baiocchi, C. Identification of the Unknown Transformation Products Derived from Clarithromycin and Carbamazepine Using Liquid Chromatography/High-Resolution Mass Spectrometry. *Rapid Commun. Mass Spectrom.* **2012**, *26*, 1687–1704. [[CrossRef](#)]
40. Martínez-Piernas, A.B.; Nahim-Granados, S.; Polo-López, M.I.; Fernández-Ibáñez, P.; Murgolo, S.; Mascolo, G.; Agüera, A. Identification of Transformation Products of Carbamazepine in Lettuce Crops Irrigated with Ultraviolet-C Treated Water. *Environ. Pollut.* **2019**, *247*, 1009–1019. [[CrossRef](#)] [[PubMed](#)]
41. Franz, S.; Falletta, E.; Arab, H.; Murgolo, S.; Bestetti, M.; Mascolo, G. Degradation of Carbamazepine by Photo(Electro)Catalysis on Nanostructured TiO₂ Meshes: Transformation Products and Reaction Pathways. *Catalysts* **2020**, *10*, 169. [[CrossRef](#)]
42. Buchicchio, A.; Bianco, G.; Sofò, A.; Masi, S.; Caniani, D. Biodegradation of Carbamazepine and Clarithromycin by *Trichoderma Harzianum* and *Pleurotus Ostreatus* Investigated by Liquid Chromatography—High-Resolution Tandem Mass Spectrometry (FTICR MS-IRMPD). *Sci. Total Environ.* **2016**, *557–558*, 733–739. [[CrossRef](#)]
43. Castro, G.; Casado, J.; Rodríguez, I.; Ramil, M.; Ferradás, A.; Cela, R. Time-of-Flight Mass Spectrometry Assessment of Fluconazole and Climbazole UV and UV/H₂O₂ Degradability: Kinetics Study and Transformation Products Elucidation. *Water Res.* **2016**, *88*, 681–690. [[CrossRef](#)]
44. Schymanski, E.L.; Jeon, J.; Gulde, R.; Fenner, K.; Ruff, M.; Singer, H.P.; Hollender, J. Identifying Small Molecules via High Resolution Mass Spectrometry: Communicating Confidence. *Environ. Sci. Technol.* **2014**, *48*, 2097–2098. [[CrossRef](#)] [[PubMed](#)]
45. Nélieu, S.; Shankar, M.V.; Kerhoas, L.; Einhorn, J. Phototransformation of Monuron Induced by Nitrate and Nitrite Ions in Water: Contribution of Photonitration. *J. Photochem. Photobiol. A Chem.* **2008**, *193*, 1–9. [[CrossRef](#)]
46. Boix, C.; Ibáñez, M.; Sancho, J.V.; Parsons, J.R.; de Voogt, P.; Hernández, F. Biotransformation of Pharmaceuticals in Surface Water and during Waste Water Treatment: Identification and Occurrence of Transformation Products. *J. Hazard. Mater.* **2016**, *302*, 175–187. [[CrossRef](#)] [[PubMed](#)]
47. Shah, R.P.; Sahu, A.; Singh, S. Identification and Characterization of Degradation Products of Irbesartan Using LC–MS/TOF, MSn, on-Line H/D Exchange and LC–NMR. *J. Pharm. Biomed. Anal.* **2010**, *51*, 1037–1046. [[CrossRef](#)] [[PubMed](#)]
48. Rayaroth, M.P.; Aravind, U.K.; Aravindakumar, C.T. Photocatalytic Degradation of Lignocaine in Aqueous Suspension of TiO₂ Nanoparticles: Mechanism of Degradation and Mineralization. *J. Environ. Chem. Eng.* **2018**, *6*, 3556–3564. [[CrossRef](#)]
49. Lege, S.; Sorwat, J.; Yanez Heras, J.E.; Zwiener, C. Abiotic and Biotic Transformation of Torasemide—Occurrence of Degradation Products in the Aquatic Environment. *Water Res.* **2020**, *177*, 115753. [[CrossRef](#)] [[PubMed](#)]